First publ. in: PNAS (Proceedings of the National Academy of Sciences) 101 (2004), 32, pp. 11571-11576

Crystal structure of pyrogallol–phloroglucinol transhydroxylase, an Mo enzyme capable of intermolecular hydroxyl transfer between phenols

Albrecht Messerschmidt*†, Holger Niessen‡, Dietmar Abt‡, Oliver Einsle*§, Bernhard Schink‡, and Peter M. H. Kroneck‡†

*Abteilung Strukturforschung, Max-Planck-Institut für Biochemie, Am Klopferspitz 18, 82152 Martinsried, Germany; ‡Mathematisch-Naturwissenschaftliche Sektion, Fachbereich Biologie, Universität Konstanz, Postfach M665, 78457 Konstanz, Germany; and §Abteilung für Molekulare Strukturbiologie, Institut für Mikrobiologie und Genetik, Georg-August-Universität Göttingen, Justus-von-Liebig-Weg 11, 37077 Göttingen, Germany

Communicated by Helmut Beinert, University of Wisconsin, Madison, WI, June 24, 2004 (received for review March 23, 2004)

The Mo enzyme transhydroxylase from the anaerobic microorganism *Pelobacter acidigallici* catalyzes the conversion of pyrogallol to phloroglucinol. Such trihydroxybenzenes and their derivatives represent important building blocks of plant polymers. None of the transferred hydroxyl groups originates from water during transhydroxylation; instead a cosubstrate, such as 1,2,3,5-tetrahydroxybenzene, is used in a reaction without apparent electron transfer. Here, we report on the crystal structure of the enzyme in the reduced Mo(IV) state, which we solved by single anomalous-diffraction technique. It represents the largest structure (1,149 amino acid residues per molecule, 12 independent molecules per unit cell), which has been solved so far by single anomalous-diffraction technique. Tranhydroxylase is a heterodimer, with the active Mo–molybdopterin guanine dinucleotide (MGD)$_2$ site in the α-subunit, and three [4Fe—4S] centers in the β-subunit. The latter subunit carries a seven-stranded, mainly antiparallel β-barrel domain. We propose a scheme for the transhydroxylation reaction based on 3D structures of complexes of the enzyme with various polyphenols serving either as substrate or inhibitor.

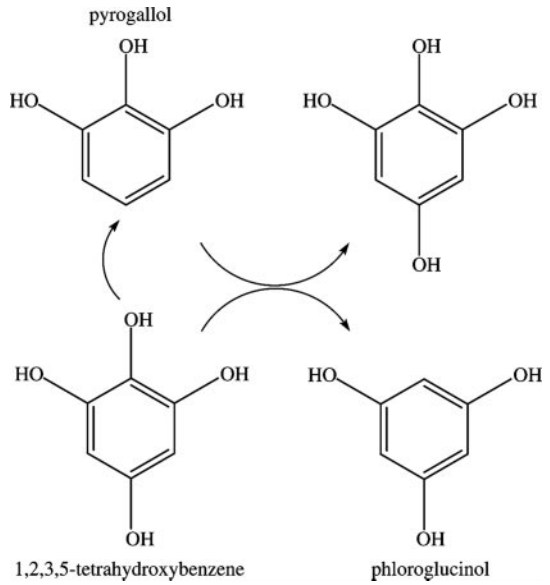

Scheme 1. Proposed role of 1,2,3,5-tetrahydroxybenzene as cosubstrate in the TH reaction.

The strictly anaerobic bacterium *Pelobacter acidigallici* ferments gallic acid, pyrogallol, phloroglucinol, or phloroglucinol carboxylic acid to three molecules of acetate (plus CO_2) (1–3). A key enzyme in the fermentation pathway is pyrogallol–phloroglucinol transhydroxylase (TH), which converts pyrogallol to phloroglucinol in the absence of O_2. In cell-free extracts, the reaction requires 1,2,3,5-tetrahydroxybenzene as a cosubstrate, and maximal reaction rates (equivalent to physiological reaction rates) were obtained in the presence of 1 mM tetrahydroxybenzene. The proposed reaction scheme is shown in Scheme 1. The transfer of the hydroxyl group from the cosubstrate to the pyrogallol is indicated by an arrow. Although this transfer between two aromatic compounds does not represent a net redox reaction, the substrate pyrogallol is oxidized in position 5, and the cosubstrate 1,2,3,5-tetrahydroxybenzene is reduced in position 2. Incubation experiments with $^{18}OH_2$ showed that there is no O exchange with water and that the hydroxyl groups are transferred only between the phenolic substrates (4).

TH is a cytoplasmic Mo enzyme consisting of a large α-subunit of 875 amino acid residues and a small β-subunit of 274 amino acid residues. The α-subunit hosts the Mo ion coordinated to two molybdopterin guanine dinucleotide (MGD) cofactors. The β-subunit holds three [4Fe—4S] clusters. Based on the nucleotide sequence of its coding gene (5) TH belongs to the DMSO reductase (DMSOR) family. The first crystal structure for a protein of this family was the one reported for DMSOR from *Rhodobacter sphaeroides* (6). Members of the DMSOR family share the Mo-containing α-subunit, such as DMSOR (6–8), formate dehydrogenase (FDH)-H (9), and dissimilatory nitrate reductase (NIR) (10), but may also have one or two additional small subunits as observed in arsenite oxidase (11) and in tungsten-containing FDH-T (12) (α- and β-subunits), and in NIR A (NARGHI) (13) and FDH-N (14) (α-, β-, and γ-subunits). The only protein ligand to the Mo ion is either a Ser (DMSOR, TH), Cys (dissimilatory NIR), Asp (NIR A), or seleno-Cys (FDHs). Arsenite oxidase is unique in having no covalent linkage between the protein and the Mo atom (11). All of these enzymes function as typical Mo hydroxylases, with the Mo ion cycling between Mo(IV) and Mo(VI) during catalytic turnover. Here, we report the crystal structures of TH from *P. acidigallici* in complex with acetate, pyrogallol, and 1,2,4-trihydroxybenzene (INH) at resolutions of 2.35, 2.20, and 2.00 Å, respectively.

Materials and Methods

Protein Production and Crystallization. *P. acidigallici* strain MaGal 2 (GenBank accession no. DSM 2377) was grown anaerobically in a sulfide-reduced and bicarbonate-buffered saltwater mineral medium. The culture was fed three times with 7 mM gallic acid during growth. Transhydroxylase was purified under air at

Abbreviations: TH, pyrogallol–phloroglucinol transhydroxylase; MGD, molybdopterin guanine dinucleotide; FDH, formate dehydrogenase; NIR, nitrate reductase; DMSOR, DMSO reductase; INH, 1,2,4-trihydroxybenzene.

Data Deposition: The atomic coordinates and structure factors have been deposited in the Protein Data Bank, www.rcsb.org (PDB ID codes 1TI2/1VLD, 1TI4/1VLE, and 1TI6/1VLF for native enzyme, pyrogallol complex, and inhibitor complex, respectively).

†To whom correspondence may be addressed. E-mail: peter.kroneck@uni-konstanz.de or messersc@biochem.mpg.de.

BIOCHEMISTRY

Table 1. Data collection and refinement statistics

	Native	Native/SAD	TH complex	INH–TH complex
Space group	P1	P1	P1	P1
Unit cell				
a, Å	174.02	172.96	172.47	172.57
b, Å	179.64	178.58	178.14	178.44
c, Å	181.22	179.91	179.05	179.67
α, °	63.38	63.95	64.11	63.83
β, °	63.98	64.32	64.45	64.40
γ, °	64.90	65.03	65.10	65.04
Wavelength, Å	1.7426	1.73647	1.05	0.9393
Resolution range,* Å	38.63–2.35 (2.39–2.35)	25–2.8 (2.95–2.80)	25–2.2 (2.32–2.20)	25–2.0 (2.11–2.00)
Measurements	1,733,679	2,895,987	2,639,960	3,432,221
Unique reflections	635,960	378,146	814,421	1,084,767
Completeness*	90.1 (87.2)	92.4 (68.7)	96.9 (96.1)	96.6 (92.0)
Multiplicity*	2.3 (2.2)	7.6 (6.9)	3.2 (3.2)	3.2 (2.7)
I/σ, I*	7.0 (1.2)	4.9 (2.1)	5.1 (1.4)	4.0 (1.9)
R_{merge},*† %	13.4 (60.0)	12.7 (28.8)	14.0 (51.5)	12.0 (34.0)
R_{anom},*‡ %	—	5.7 (12.9)	—	—
Phasing power§	—	1.12/0.578	—	—
Mean FOM¶	—	0.22/0.56	—	—
R_{cryst}/R_{free},‖ %	19.9/25.4	—	17.9/22.4	17.2/20.2
No. of atoms				
Nonhydrogen protein (altconf)	110,412 (240)	—	110,172	110,172
PGD	1,128	—	1,128	1,128
Mo ions	12	—	12	12
Fe ions	144	—	144	144
Ca ions	24	—	24	24
Inorganic S	144	—	144	144
Ligand	48**	—	108	120
Water molecules	10,157	—	10,089	10,091
Average *B*-factor (all atoms), Å^2	33.3	—	21.1	18.8
rms deviation				
Bond lengths, Å	0.008	—	0.008	0.008
Angles, °	1.9	—	1.8	1.8

SAD, single-wavelength anomalous diffraction; FOM, figure of merit; PGR, pterin guanine dinucleotide.

*Values in parentheses are for the highest-resolution shell.

†R_{merge} $(I) = \Sigma\Sigma|I(h)_i - \langle I(h)\rangle|/\Sigma\Sigma I(h)_i$, where $I(h)_i$ is the observed intensity in the ith source and $\langle I(h)\rangle$ is the mean intensity of reflection h over all measurements of $I(h)$.

‡$R_{anom} = \Sigma|\langle I(+h)\rangle - \langle I(-h)\rangle|/\Sigma(\langle I(+h)\rangle + \Sigma\langle I(+h)\rangle)$, where $\langle I(+h)\rangle$ and $\langle I(-h)\rangle$ are the mean values of the intensities for the respective Friedel mates.

§Phasing power = rms $[F(+h) - F(-h)]$/rms residual, where $[F(+h) - F(-h)]$ is either the observed anomalous difference, which was used for the calculation of the first figure, or the calculated anomalous difference, which was used for the calculation of the second figure. The rms residual is an estimate of the remaining heavy-atom structure factor based on the anomalous differences and errors in the measurement.

¶FOM is the first figure that was obtained from SOLVE and the second figure after RESOLVE.

‖R-factors were calculated by using data $F > 0\ \sigma$, R-factor $= \Sigma_{hkl}||F_o| - |F_c||/\Sigma_{hkl}|F_o|$, where $|F_o|$ and $|F_c|$ are the observed and calculated structure factor amplitudes for reflection hk1, applied to the work (R_{cryst}) and test (R_{free}) (10% omitted from refinement) sets, respectively.

**Acetate.

278 K (15); the chromatofocusing step was omitted, which led to partial decomposition of one of the [4Fe—4S] clusters, as shown by EPR spectroscopy (16). Crystallization was done in a N_2/H_2 (95/5%) atmosphere at 18°C in sitting drops by the vapor-diffusion technique. We mixed 3 μl of protein solution containing 12 mg/ml Na-dithionite (pH 7.5, 12 equivalents) and 10% (vol/vol) additive (0.1 M sodium cacodylate, pH 6.5/1.4 M sodium acetate) with 3.5 μl of reservoir solution (0.05 M potassium phosphate, pH 7.5/20% polyethylene glycol 8000). Crystals formed over a period of 1–6 weeks and were frozen directly from the crystallization solution after adding 2,4-methylpentanediol to a final concentration of 25%. The substrate and inhibitor complexes were obtained by soaking crystals in the absence of O_2 for 15 min in cryo-buffer solution containing 5 mM pyrogallol (substrate) or 5 mM INH (inhibitor), respectively.

Structure Determination. X-ray data were collected at beam line BW6 at Deutsches Elektronensynchrotron (Hamburg, Germany) (native data set and complex structure with pyrogallol) and at beam line ID29 at the European Synchrotron Radiation Facility (Grenoble, France) (high-redundancy single-wavelength anomalous-diffraction data set and complex structure with INH). They were processed with MOSFLM (17), scaled, and further reduced by using the CCP4 suite of programs (available at www.ccp4.ac.uk) (Table 1). The native structure was solved by the single anomalous-diffraction technique using a high-redundant data set ($2 \times 360°$ rotation angle) at the maximum of the f'' of the Fe absorption edge (2.8-Å resolution). The positions

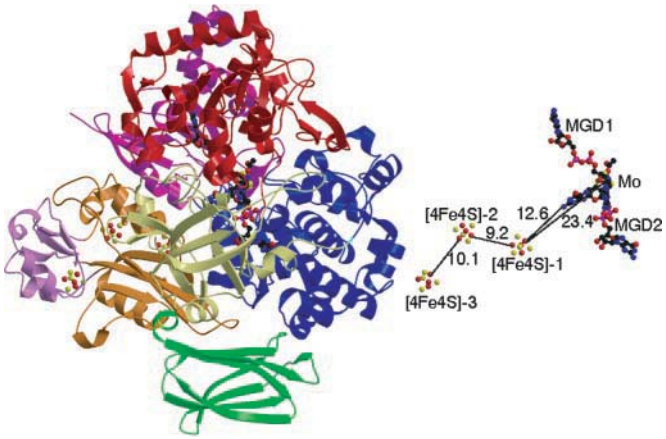

Fig. 1. Overall structure of TH. The α-subunit domains I–IV are shown in magenta, blue, red, and cream, respectively. The β-subunit domains I and II are shown in orange and pink, respectively, and domain III is shown in green. The Mo and MGD cofactors are shown as ball-and-stick models, and the three [4Fe—4S] clusters are shown as red (Fe) and yellow (S) spheres. The figure was made with BOBSCRIPT (31) and RASTER3D (32).

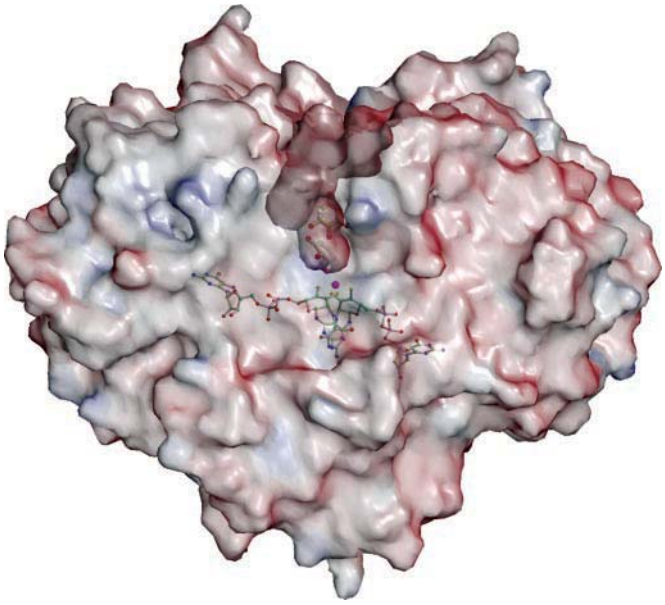

Fig. 2. Solid-surface–electrostatic potential representation of TH displaying the access channel for substrate and cosubstrate. The electrostatic surface potentials are contoured from −10 (red) to 10 K_BT/e (blue). The figure was made with GRASP (34) and RASTER3D (32).

of 33 of the 36 [4Fe—4S] clusters present in the P1 triclinic unit cell (12 heterodimers per unit cell) could be located by using the Shake-and-Bake procedure (18). Initial phases for both hands were calculated with SHARP (19), and the residual three cluster positions and the correct hand for the phase calculation could be determined. The individual Fe positions within the clusters could not be resolved because of the actual resolution. The Fe positions were entered into an "analyse" run in SOLVE (20), and noncrystallographic symmetry operators were determined in RESOLVE (21), followed by solvent flattening of the electron density. The resulting electron-density map clearly showed secondary structure elements. This electron-density map was 12-fold averaged by using AVE (22). Model building was done in this improved map by using program O (available at http://x-ray.bmc.uu.se/alwyn), and refinement was performed by using CNS (available at http://cns.csb.yale.edu) (23) with the native data set collected at BW6 (2.35-Å resolution, $R_{cryst} = 0.199$, $R_{free} = 25.4$). Both complex structures were solved with difference Fourier technique by using the structural model of native TH and refined with CNS (pyrogallol complex: 2.20-Å resolution, $R_{cryst} = 0.179$, $R_{free} = 22.4$; INH–TH complex: 2.00-Å resolution, $R_{cryst} = 0.172$, $R_{free} = 20.2$) (for all refinements, see Table 1). The structural superpositions were made with LSQMAN (24).

Results and Discussion

Overall Structure. The crystal structure shows that TH is a heterodimer of ≈75 × 60 × 83 Å, with the α- and β-subunits consisting of four and three domains, respectively, and the relevant metal and MGD cofactors (Fig. 1). The α-subunit (875 residues) is in the middle of the range from 755 residues for NIR and 982 residues for FDH-N, and it does not contain a fifth domain as in FDH-N and FDH-T. The four domains are similar to the domains of the other DMSOR family organized around the MGD cofactors (Figs. 5*A* and 6*A*, which are published as supporting information on the PNAS web site). The fold of TH is completely different between the secondary structure elements β3 and α1, β6 and β7, β15 and α23, α23 and β19, β22 and β23, α35 and β25, and β25 and β26, and it concerns ≈250 amino acid residues. Many of them take part in the formation of the substrate and cosubstrate binding sites, which are accessible from the solvent through a narrow channel (Fig. 2). It contains three cis peptides at Phe A166, Pro A483, and Pro A670. The β-subunit consists of three domains and has one cis peptide at Pro B57 (Figs. 5*B* and 6*B*). Domains I and II are ferredoxin-like domains, which together superimpose well with the relevant ferredoxin domains of the β-subunits of FDH-T (132 Cα atoms, rms deviation 1.15 Å) and FDH-N T (144 Cα atoms, rms deviation 1.13 Å). Domain I holds two and domain II holds one Fe–S cluster as in FDH-T, in contrast to FDH-N, which has two clusters in both domains. Domain III, starting at residue B190, is folded in a seven-stranded mainly antiparallel β-barrel. A search with domain III for related 3D structures in the DALI server (25) revealed the same fold for transthyretin (prealbumin) (26) and a closely related one for tenascin (third fibronectin type III repeat) (27). The latter is a cell-adhesion protein, and TH may be associated with the cytoplasmic membrane via this domain.

Active Site and Complex Structures. The active site of TH is located in the α-subunit and includes the Mo-binding site, with six ligands arranged in a distorted trigonal pyramid. The coordination of the Mo ion is similar to that in DMSOR (28) (Fig. 3*A*). There are four S ligands from both MGD moieties (bond distances between 2.39 and 2.46 Å), OG from Ser A175 (1.85 Å), and an O from an acetate molecule (1.78 Å), which originates from the crystallization buffer. In the acetate-free native structure, this space is probably filled by a hydroxyl or water molecule. The Mo ion should be in the Mo(IV) oxidation state because (*i*) the protein was crystallized under the strict exclusion of O_2 under N_2/H_2 (95/5%), and (*ii*) the crystallization buffer had an excess of sodium dithionite as reductant. The Mo (V) oxidation state has been detected by EPR (signal at $g_{av} \approx 1.98$) in the enzyme as isolated in the presence of air (16). The side chain of Tyr A560 adopts two different conformations and locks the active site if it is in the right conformation shown in Fig. 3*A*. In the crystal structure of the pyrogallol–TH substrate complex, the pyrogallol binds with its O1 oxygen to the Mo (Fig. 3*B*, 2.4-Å bond distance) and replaces the acetate or the hydroxyl or water group in the acetate-free enzyme. This reaction is catalyzed by His A144 (NE2 in H bond distance to O1 of pyrogallol), which acts as general base. The other part of the Mo coordination remains unaltered, with similar bond distances as in the native structure. Carbon C1 of pyrogallol is in the sp^3 state represented by the position of O1 above the plane of the pyrogallol benzene

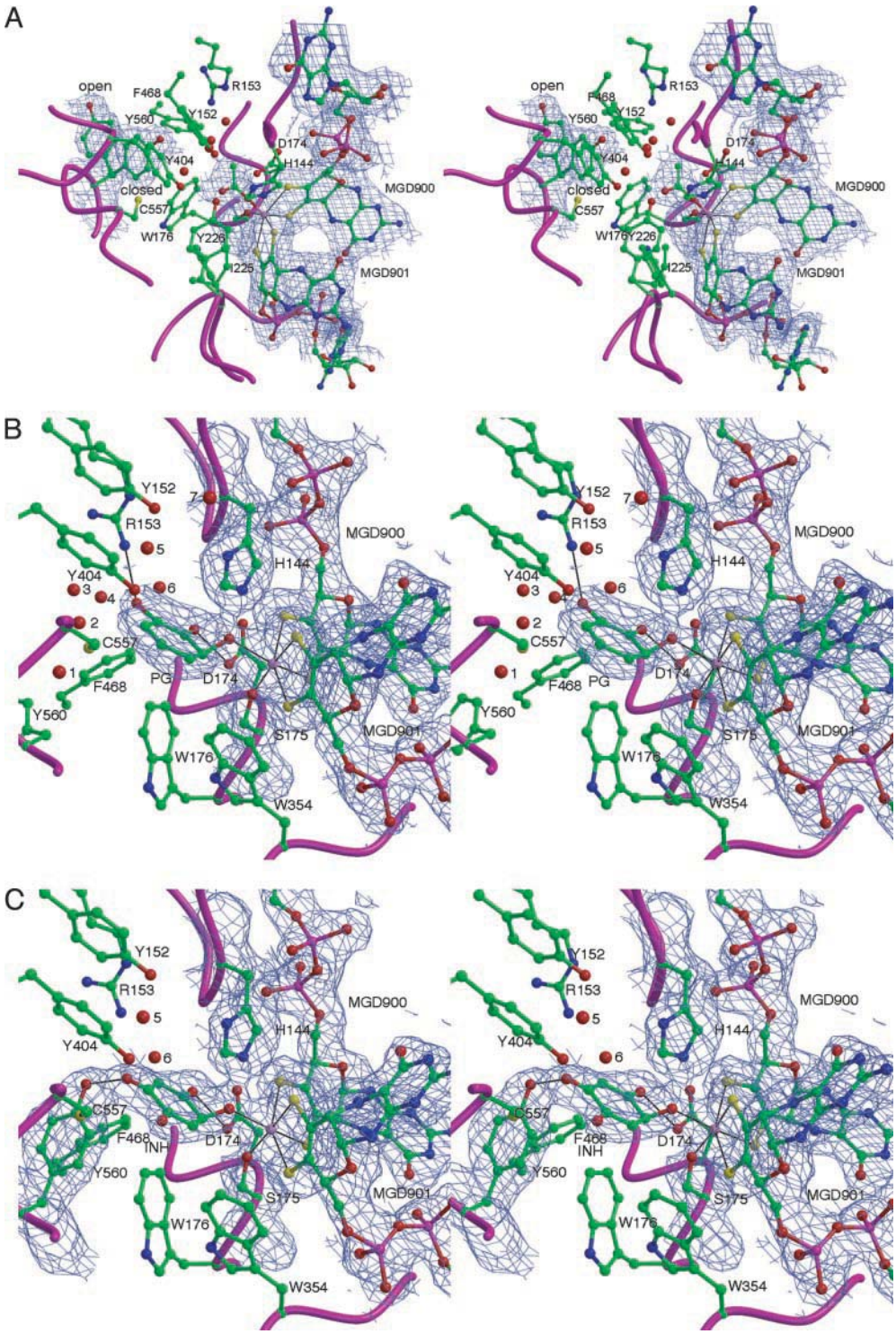

Fig. 3. Stereo image of the active site in TH plus $2F_O–F_C$ electron density contoured at 1 σ for selected residues. (*A*) Native TH with bound acetate molecule. (*B*) TH in complex with substrate pyrogallol (PG). (*C*) TH in complex with INH. The images were made with BOBSCRIPT (31) and RASTER3D (32).

ring. O2 is H bonded to OE2 of Asp A174 and O3 to NH2 of Arg A153. The Mo and the side chain functions of Asp A174 and Arg A153 are the recognition sites for the substrate. The side chain of Tyr A560 is in the open conformation and allows substrate binding. The space of the alternate conformation has been occupied by water molecules 1–3. The side chains of Tyr A404 and Tyr A152 are situated on top of the pyrogallol molecule. Their phenol rings are stacked parallel to each other. The OH group of Tyr A404 and the SG of Cys A557 are in H-bonding distances to C5 of pyrogallol, and they may play a role as general base in catalysis of the hydroxyl transfer from the cosubstrate to the substrate. The space below the benzene ring of pyrogallol is lined by hydrophobic residues, such as Trp A176, Trp A354, and Phe A468. They create the hydrophobic surface region for binding of the hydrophobic part of the substrate molecule in the active site.

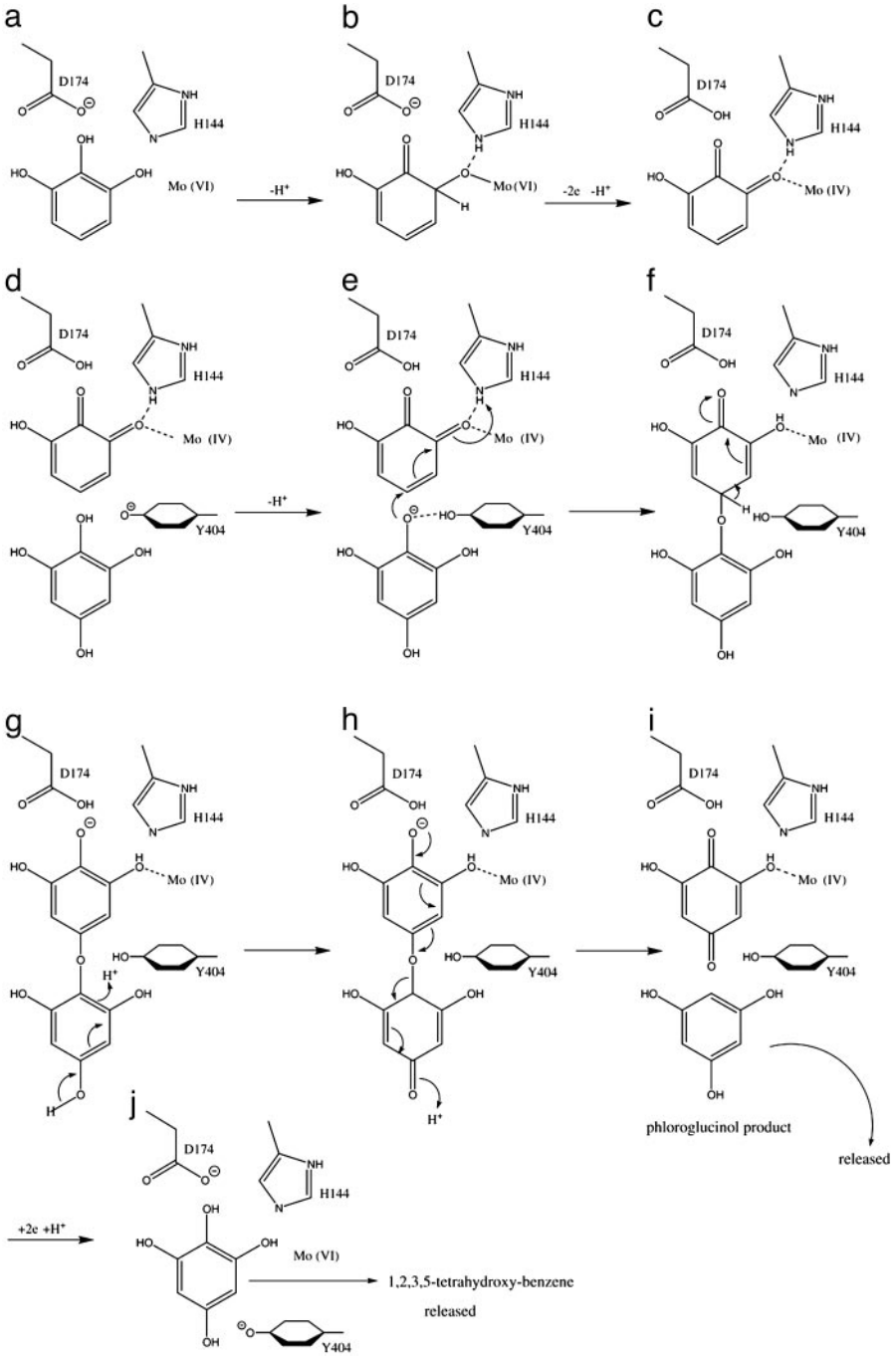

Scheme 2. Proposed reaction scheme for TH.

The crystal structure of the pyrogallol–TH inhibitor complex shows the INH molecule bound with its O5 atom coordinated to the Mo (Fig. 3*C*, 2.35-Å bond distance). The other part of the Mo coordination is identical to the native structure of the pyrogallol–TH complex with similar bond distances. The side chain of Tyr A560 is in the closed conformation, and the OH is bound to O2 of the inhibitor. O4 is H bonded to Asp A174, and O1 points into the direction of the side chain of Cys A577. Arg A153 cannot contact the inhibitor molecule because the corresponding OH function is missing in the inhibitor.

Mechanistic Aspects. Three different proposals for the catalytic mechanism of TH have been made (29). The first mechanism includes 1,2,3,5-tetrahydroxybenzene as cosubstrate through a diphenylether intermediate, and the transferred hydroxyl does not originate from the solvent. The other two mechanisms function without cosubstrate and involve a rotation of the substrate in the active site during catalysis, which is denoted as "Umpolung." The hydroxyl stems from the solvent in this mechanism. The 3D structure of TH supports the participation of a cosubstrate in the mechanism. Fig. 4 shows a schematic representation of the active site with bound pyrogallol as found in the relevant complex structure and manually docked cocatalyst. It adopts the position of the phenyl ring of Tyr A560 when it is in the closed conformation and can form several H bonds with the protein and pyrogallol (dashed lines in Fig. 4). O2, the hydroxyl to be transferred to C5 of

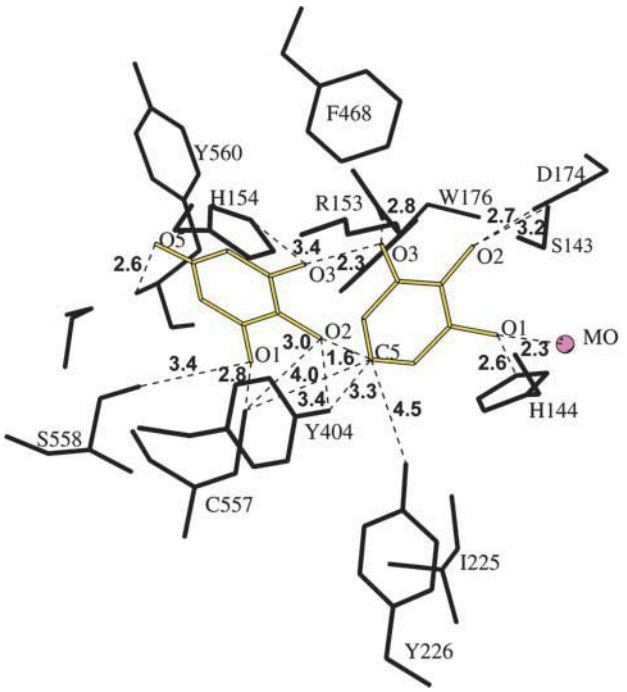

Fig. 4. Schematic representation of the active site with bound pyrogallol and manually docked cocatalyst 1,2,3,5-tetrahydroxybenzene, both of which are shown in yellow.

pyrogallol, is in close proximity to this atom. Tyr A404 is the most probable candidate to act as general base in this transfer reaction because its OH group lies at appropriate distances to both atoms (3.4 Å to O2 and 3.3 Å to C5), but Cys A557 could also play this role (distances of 3.0 and 4.0 Å, respectively). This mechanism is in line with the experimental findings that 1,2,3,5-tetrahydroxybenzene is needed to start the reaction and that the transferred hydroxyl does not come from the solvent. Based on the structural data, the proposed mechanism (Scheme 2) involves Asp A174, His A144, Tyr A404, and the Mo as catalytic residues and goes through reaction intermediates, as shown in figure 7 in ref. 29. Pyrogallol enters the active site first (Scheme 2*a*) and is bound (Scheme 2*b*) as in the pyrogallol–TH complex structure. The Mo is in the +VI oxidation state. Asp A174, Tyr A404, and His A144 are in the deprotonated state. His A144 abstracts the proton from O1, thus promoting its binding to Mo(VI). Mo oxidizes the enol tautomer of pyrogallol to the orthoquinone form and gets reduced to Mo (IV) (Scheme 2*c*). Tyr A404 abstracts a proton from O2 (Scheme 2*d*). Subsequently, the O^- of the cosubstrate attacks the C5 of pyrogallol in a nucleophilic manner. A bridging bond from O2 to C5 of the pyrogallol is formed, causing the flip of one double bond in the ring system and the nucleophilic attack of the double bond between C3 and O3 of pyrogallol at the proton of NE2 of His A144 (Scheme 2*e*), resulting in the structure shown in Scheme 2*f*. The indicated rearrangements lead to formation of diphenylether (Scheme 2*f*). Going through chemically plausible intermediates and reactions (Scheme 2 *g* and *h*), the covalent adduct between substrate and cosubstrate can be cleaved to form the product phloroglucinol and the quinone form of tetrahydroxybenzene (Scheme 2*i*). Reduction of the quinone form of tetrahydroxybenzene by Mo(IV) and transfer of the respective protons from Asp A174 and Tyr A404 would close the catalytic cycle (Scheme 2*j*).

Role of Fe–S Clusters. The role of the [4Fe—4S] clusters in the β-subunit remains unclear. Their nearest Fe–Fe distances are 10.1 and 9.2 Å (Fig. 1), which would be suitable for an efficient electron transfer. However, the nearest Fe–Mo and Fe–MGD group distances are 23.4 and 12.6 Å, respectively. Compared with the distance between Fe and the pterin cofactor, the distance of 23.4 Å appears to be rather long for an effective electron transfer between the nearest [4Fe—4S] cluster and the Mo ion. However, a closest distance of 12.4 Å from a [4Fe—4S] cluster to the methyl group C8M of flavin-adenine dinucleotide (FAD) has been found in adenylylsulfate reductase from *Archaeoglobus fulgidus* (30). Efficient electron transfer seems to be enhanced here by a strictly conserved Trp residue located between the two cofactors and in van der Waals contact to both centers. No such aromatic residue between the [4Fe—4S] cluster and the MGD group is found in TH.

The catalyzed reaction of TH is a net nonredox reaction and does not require redox equivalents from outside. Therefore, it lacks the [4Fe—4S] cluster in the α-subunit, which would allow an effective electron transfer between the Mo redox center and the [4Fe—4S] clusters of the β-subunit, as observed in FDH-T, FDH-N, and NARGHI. This finding might suggest that TH evolved from such enzymes and carries the β-subunit as a relict without catalytic function in the transhydroxylase reaction but uses the fibronectin-like domain for membrane association.

We thank R. Huber for supporting this project and giving valuable suggestions; M. Augustin, G. Bourenkov, and H. D. Bartunik for assistance with data collection at BW6 of Deutsche Elektronensynchrotron in Hamburg; the European Synchrotron Radiation Facility in Grenoble for provision of synchrotron radiation facilities; and A. Thompson and G. Leonard (ID29) for assistance. H.N., B.S., and P.M.H.K. were supported by the Deutsche Forschungsgemeinschaft priority program "Radicals in Enzymatic Catalysis."

1. Schink, B. & Pfennig, N. (1982) *Arch. Microbiol.* **133,** 195–201.
2. Brune, A. & Schink, B. (1990) *J. Bacteriol.* **172,** 1070–1076.
3. Brune, A. & Schink, B. (1992) *Arch. Microbiol.* **157,** 417–424.
4. Reichenbecher, W. & Schink, B. (1999) *Biochim. Biophys. Acta* **19,** 245–253.
5. Baas, D. & Rétey, J. (1999) *Eur. J. Biochem.* **265,** 896–901.
6. Schindelin, H., Kisker, C., Hilton, J., Rajagopalan, K. V. & Rees, D. C. (1996) *Science* **272,** 1615–1621.
7. McAlpine, A. S., McEwan, A.G., Shaw, A. L. & Bailey, S. (1997) *J. Biol. Inorg. Chem.* **2,** 690–701.
8. Schneider, F., Löwe, J., Huber, R., Schindelin, H., Kisker, C. & Knäblein, J. (1996) *J. Mol. Biol.* **263,** 53–69.
9. Boyington, J. C., Gladyshev, V. N., Khangulov, S. V., Stadtman, T. C. & Sun, P. D. (1997) *Science* **275,** 1305–1308.
10. Dias, J. M., Than, M. E., Humm, A., Huber, R., Bourenkov, G. P., Bartunik, H. D., Bursakov, S., Calvete, J., Caldeira, J., Carneiro, C., *et al.* (1999) *Structure (London)* **7,** 65–79.
11. Ellis, P. J., Conrads, T., Hille, R. & Kuhn, P. (2003) *Structure (London)* **9,** 125–132.
12. Raaijmakers, H., Macieira, S., Dias, J. M., Teixeira, S., Bursakov, S., Huber, R., Moura, J. J. G., Moura, I. & Romao, M. J. (2002) *Structure (London)* **10,** 1261–1272.
13. Bertero, M. G., Rothery, R. A., Palak, M., Hou, C., Lim, D., Blasco, F., Weiner, J. H. & Strynadka, N. C. J. (2003) *Nat. Struc. Biol.* **10,** 681–687.
14. Jormakka, M., Törnroth, S., Byrne, B. & Iwata, S. (2002) *Science* **295,** 1863–1868.
15. Reichenbecher, W., Brune, A. & Schink, B. (1994) *Biochim. Biophys. Acta* **1204,** 217–224.
16. Kisker, C., Schindelin, H., Baas, D., Rétey, J., Meckenstock, R. U. & Kroneck, P. M. H. (1999) *FEMS Microbiol. Rev.* **22,** 503–521.
17. Leslie, A. G. W. (1999) *Acta Crystallogr. D* **55,** 1696–1702.
18. Xu, H. L. Hauptmann, H. A. & Weeks, C. M. (2002) *Acta Crystallogr. D* **58,** 90–96.
19. La Fortelle, E. D., Irwin, J. J. & Bricogne, G. (1997) *Crystallogr. Comput.* **7,** 1–9.
20. Terwilliger, T. C. & Berendzen, J. (1999) *Acta Crystallogr. D* **55,** 849–861.
21. Terwilliger, T. C. (2000) *Acta Crystallogr. D* **56,** 965–972.
22. Jones, T. A. (1992) in *Molecular Replacement (CCP4*), eds. Dodson, E. J., Gover, S. & Wolf, W. (Darebury Laboratory, Warrington, U.K.), pp. 99–105.
23. Brünger, A. T., Adams, P. D., Clore, G. M., Delano, W. L., Gros, P., Grosse-Kunstleve, R. W., Jiang, J.-S., Kszewski, J., Nilges, M., *et al.* (1998) *Acta Crystallogr. D* **54,** 905–921.
24. Kleywegt, G. J. & Jones, T. A. (1994) *ESF/CCP4 Newslett.* **31,** 9–14.
25. Holm, L. & Sander, C. (1993) *J. Mol. Biol.* **233,** 123–138.
26. Hamilton, J. A., Steinrauf, L. K., Braden, B. C., Liepnieks, J., Benson, M. D., Holmgren, G., Sandgren, O. & Steen, L. (1993) *J. Biol. Chem.* **268,** 2416–2424.
27. Leahy, D. J., Hendrickson, W. A., Aukhil, I. & Erickson, H. P. (1992) *Science* **258,** 987–991.
28. Li, H.-K., Temple, C., Rajagopalan, K. V. & Schindelin, H. (2000) *J. Am. Chem. Soc.* **122,** 7673–7680.
29. Hille, R., Rétey, J., Bartlewski-Hof, U., Reichenbecher, W. & Schink, B. (1999) *FEMS Microbiol. Rev.* **22,** 489–501.
30. Fritz, G., Roth, A., Schiffer, A., Büchert, T., Bourenkov, G., Bartunik, H. D., Huber, H., Stetter, K. O., Kroneck, P. M. H. & Ermler, U. (2002) *Proc. Natl. Acad. Sci. USA* **99,** 1836–1841.
31. Esnouf, R. M. (1997) *J. Mol. Graphics Model.* **15,** 132–134.
32. Merrit, E. A. & Murphy, M. E. P. (1994) *Acta Crystallogr. B* **50,** 869–873.
33. Barton, G. J. (1993) *Protein Eng.* **6,** 37–40.
34. Nicolls, A., Sharp, K.A. & Honig, B. (1991) *Proteins Struct. Funct. Genet.* **11,** 281–296.